School of Biomedical Engineering, Science, and Health Systems

Flexural Vibrations and Resonance of Piezoelectric Cantilevers with a Nonpiezoelectric Extension

Zuyan Shen, Wan Y. Shih, and Wei-Heng Shih

***Abstract*—A piezoelectric cantilever (PEC) is a flexural transducer consisting of a piezoelectric layer [e.g., lead zirconate titanate (PZT)] bonded to a nonpiezoelectric layer (e.g., stainless steel). A PEC with a thin nonpiezoelectric extension has two distinctive sections, each with a different thickness, different axial density, and elastic-modulus profiles and has been increasingly used as an in-situ biosensor. It has the advantages of dipping only the nonpiezoelectric extension part in an aqueous solution without electrically insulating the piezoelectric section as well as serving as the bonding pad for receptor immobilization. In this study, we examined the effect of the thin nonpiezoelectric extension on the flexural resonance spectrum and resonance vibration waveforms of PEC; in particular, how the length ratio between the piezoelectric section and the nonpiezoelectric extension section affects the resonance frequencies and resonance peak intensities of PEC. Theoretical resonance frequencies and resonance vibration waveforms were obtained using an analytical transcendental equation we derived by solving the flexural wave equation. Both experimental and theoretical results showed that the two-section structure distorted the flexural vibration waveforms from those of PEC without an extension. As a result, the higher-mode resonance peaks of PEC with a nonpiezoelectric extension could be higher than the first resonance peak due to the two-section structure. With PEC that has a piezoelectric section of 0.25-mm thick PZT bonded to 0.07 mm thick stainless steel of various length l_1 and a 0.07-mm thick nonpiezoelectric extension of length l_2, we showed that the first-mode-to-second-mode resonance peak intensity ratio had a maximum of 5.6 at $l_1/l_2 = 0.75$ and the first-mode-to-second-mode resonance frequency ratio a minimum of 2.2 at $l_1/l_2 = 1.8$. These findings will undoubtedly help optimize the design and performance of PEC.**

I. Introduction

A piezoelectric cantilever (PEC) is a flexural oscillator consisting of a piezoelectric layer [e.g., lead zirconate titanate (PZT)] bonded to a nonpiezoelectric layer, e.g., stainless steel or SiO_2. Figs. 1(a) and (b) schematically show a PEC without and with a nonpiezoelectric extension, respectively. The latter represents a cantilever with two distinctive sections, each with a different thickness and different density and elastic-modulus profiles. They both are used in biological [1]–[5] and chemical [6]–[12] detection. The nonpiezoelectric extension also may be narrower than the piezoelectric section [13]. Mechanical bending oscillations can be generated by applying a small alternating current (AC) voltage (< 1 V) across the thickness of the piezoelectric layer via the converse piezoelectric effect, which in turn induces a measurable piezoelectric voltage in phase with the applied voltage by the direct piezoelectric effect. A piezoelectric cantilever's mechanical resonance frequency and resonance peak intensity can be detected easily by monitoring the maximum in the real part or phase angle of the complex electrical impedance versus frequency spectra. Monitoring a cantilever's resonance frequency has many applications. In mass detection, a piezoelectric cantilever's resonance frequency shift is measured to quantify the small mass attached to the cantilever surface [14]. In liquid property characterization, both the resonance peak frequency and the resonance peak width of a piezoelectric cantilever inserted in the liquid are measured to simultaneously determine the liquid's viscosity and density [15]. In liquid-solid transition detection, an abrupt resonance frequency shift with respect to temperature is measured to identify the transition [16]. For biological and chemical detection [1]–[10], receptors selective to a target analyte are immobilized on the cantilever surface, detection of target analytes binding to the receptors on the cantilever surface is accomplished by monitoring a cantilever's resonance frequency shift. In dynamic scanning force microscopy applications, a force gradient is detected by monitoring the impedance change of a cantilever operated at its natural resonance frequency [17]. Compared to silicon-based microcantilever resonators that require an external actuator for driving and an external optical system for detection, PEC oscillators have the advantage that they can electrically self-excite and self-detect with the actuator, the resonator, and the detector all in one device. Because silicon-based microcantilevers rely on an external piezoelectric actuator located at the base of the cantilever [18], [19], the generated oscillations are insufficient to withstand damping in water [18]. In contrast, with a built-in piezoelectric layer a piezoelectric cantilever generates strong vibrations that can withstand damping in water [8], [9], thus capable of in-water, in-situ biologi-

Manuscript received September 30, 2005; accepted August 3, 2007. This work is supported in part by the National Aeronautics and Space Administration (NASA) under Grant No. NAG2-1475, the National Institute of Health (NIH) under Grant No. 1 R01 EB000720, and the Environmental Protection Agency (EPA) under Grant No. R82960401.

Z. Shen and W.-H. Shih are with the Department of Materials Science and Engineering, Drexel University, Philadelphia, PA (e-mail: shihwh@drexel.edu).

W. Y. Shih is with the School of Biomedical Engineering, Science, and Health Systems, Drexel University, Philadelphia, PA.

Digital Object Identifier 10.1109/TUFFC.2007.494

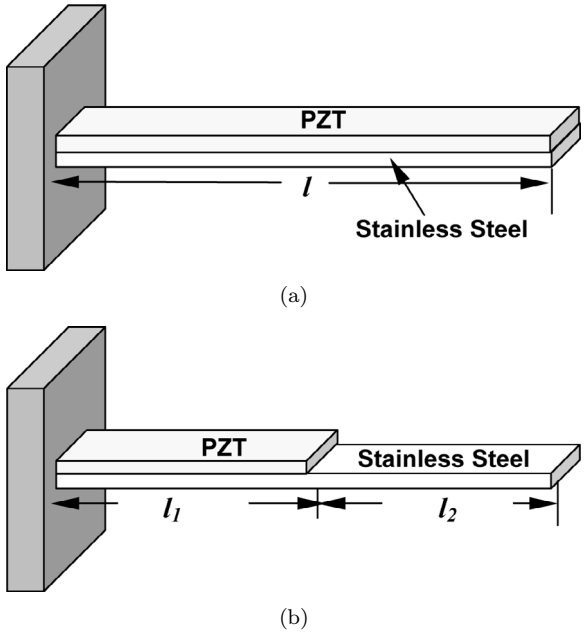

Fig. 1. A schematic of a piezoelectric cantilever of uniform thickness (a) and that of a piezoelectric cantilever with a nonpiezoelectric extension (b).

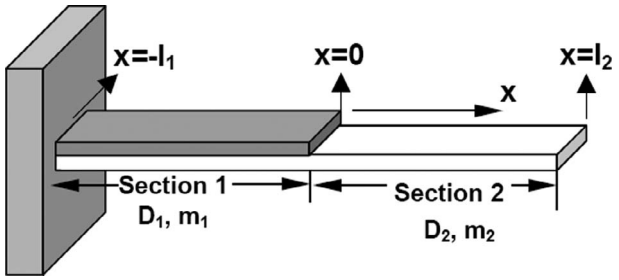

Fig. 2. A schematic of a piezoelectric cantilever with a nonpiezoelectric extension. Clearly, there are two distinctive sections, each possessing a different total thickness as well as different elastic modulus and mass density distribution in the thickness direction.

cal detection. To date, all the demonstrated in-water viscosity and biosensing applications involved piezoelectric cantilevers with a nonpiezoelectric extension. A nonpiezoelectric extension is most conveniently used as a probe to dip into any liquid for sensing applications. Although the resonance spectra of piezoelectric cantilevers of uniform thickness are well-known [20], [21] and well-characterized, very little is known for PECs with two distinctive sections. Furthermore, a PEC of uniform thickness [Fig. 1(a)] exhibits the strongest intensity in the first resonance peak and that of higher-order resonance peaks decreases with an increasing order [14]. The ratio of the n'th resonance frequency to the first resonance frequency also is predicted by the solution of the vibration wave equation of a uniform beam [14], [20], [21]. In contrast, a PEC with a nonpiezoelectric extension [Fig. 1(b)] exhibited higher resonance intensity in the second peak than in the first peak and the ratio of the frequency of the n'th resonance peak to that of the first peak was quite different from that of a uniform beam [3], [8], [9]. Little is known about how the length, width, and thickness ratios of the nonpiezoelectric extension to the piezoelectric section affect the cantilever flexural vibrations, its resonance frequencies, and resonance peak intensities.

The purpose of this paper is to investigate both experimentally and theoretically the effect of the length ratio of the nonpiezoelectric extension to the piezoelectric section on the cantilever's flexural vibrations, resonance frequencies, and resonance peak intensities. Specifically, piezoelectric cantilevers of various nonpiezoelectric extension lengths and various piezoelectric section lengths were constructed and their flexural vibration waveforms and resonance spectra were examined. Theoretically, a piezoelectric cantilever with a nonpiezoelectric extension is considered as consisting of two distinctive sections: the piezoelectric section and the nonpiezoelectric extension section. Each section possesses a different thickness, elastic modulus, and mass density distribution in the thickness direction (see Fig. 2). The cantilever's flexural vibration equation was solved analytically to obtain an analytical expression for the transcendental equation that can be used to obtain the cantilever's flexural vibration waveforms and resonance spectra numerically.

Previously, Smits and Choi [22] studied the mechanics of a piezoelectric bimorph in an applied electric field. However, their work applied only to cantilevers of uniform thickness. In a recent study, Tong and Luo [23] examined the vibrations and resonance frequencies of cantilevers partially covered by a piezoelectric actuation patch at the rear end. Although such cantilevers had the two-section geometry considered in the present study, the authors considered only cases in which the patch size was much smaller than the cantilever length, and the entire cantilever was still approximated as a uniform beam, i.e., of one thickness, one elastic modulus, and one mass density [20]. In another study, Cattafesta, III *et al.* [24] examined the flexural vibrations of a 2.52 cm long piezoelectric cantilever with a 3.81 cm long nonpiezoelectric extension at 200 Hz numerically using finite-element simulations for micropump applications. Although the authors considered the two-section geometry, their study was only for one cantilever size and focused on the effect of drag on micropump applications. The present work differs from all previous studies in that we focused on experimentally and theoretically examining the effect of the length ratio of a two-section cantilever on the cantilever's resonance frequencies and resonance peak intensities, which no previous studies had examined. In addition, the analytic transcendental equation obtained for the two-sectioned cantilevers can be solved easily to obtain the cantilever resonance frequencies and the resonance vibration waveforms. The fundamental knowledge gained by this study will undoubtedly help optimize the design and performances of piezoelectric cantilevers with a nonpiezoelectric extension.

II. Experimental

Piezoelectric cantilevers with a nonpiezoelectric extension were made by bonding a PZT layer 0.127 mm or 0.25 mm in thickness to a stainless steel layer (Alfa Aesar, Ward Hill, MA) longer than the PZT. The stainless steel was 0.05 mm to 0.1 mm in thickness. The 0.25-mm thick PZT was purchased from APC International Ltd., Mackeyville, PA; and the 0.127-mm thick PZT was purchased from Piezo Inc., Cambridge MA. The PZT layer was bonded to the stainless steel layer with a conductive epoxy (GC Conductive Epoxy, GC Electronics, Rockford, IL). The resonance spectra of the cantilever were obtained using an Agilent 4294A impedance analyzer (Agilent Technologies, Santa Clara, CA). The flexural vibration amplitude along the length of the cantilever was measured with a Keyence laser displacement meter (Keyence, Woodcliff Lake, NJ). An XYZ positioner with a 10-μm spatial resolution was used to position the displacement meter relative to the cantilever to obtain the vibration amplitude at different locations along the cantilever length. The cantilever was rigidly clamped at the end of the piezoelectric section with a steel fixture lined with a rubber buffer layer. Measurements were carried out with cantilevers of 4 mm in width. The Young's modules and densities of the PZT and stainless steel layers are listed in Table I.

TABLE I
Physical Parameters of the Cantilever with an Extension.

	PZT	Stainless steel
Density, ρ $\sim$Kg/m^3	7.5×10^3	7.8×10^3
Young's modulus, E (N/m^2)	6.1×10^{10}	20×10^{10}

III. Theory

Fig. 2 shows a schematic of a piezoelectric cantilever with a nonpiezoelectric extension with the section with the piezoelectric layer denoted as section 1 and the section with the nonpiezoelectric extension as section 2. Sections 1 and 2 have lengths of l_1 and l_2, respectively. In the current investigation, we neglected the glue layer as it is much thinner and softer than the piezoelectric layer and the nonpiezoelectric layer. Therefore, section 1 is composed of a piezoelectric layer and a nonpiezoelectric layer of thickness, t_p and t_{np}, mass density ρ_p and ρ_{np}, and Young's modulus E_p and E_{np}, respectively. Section 2 is composed of only the nonpiezoelectric layer of thickness t_{np}, mass density ρ_{np}, and Young's modulus E_{np}. With w denoting the cantilever width, the bending modulus of section 1 and that section 2 can be expressed as:

$$D_1 = w\left(\frac{E_p^2 t_p^4 + E_{np}^2 t_{np}^4 + 2E_p E_{np} t_p t_{np}\left(2t_p^2 + 2t_{np}^2 + 3t_p t_{np}\right)}{12\left(E_p t_p + E_{np} t_{np}\right)}\right), \tag{1}$$

and:

$$D_2 = w\left(\frac{E_{np} t_{np}^3}{12}\right). \tag{2}$$

The mass per unit length in section 1 and section 2 are:

$$m_1 = w\left(\rho_p t_p + \rho_{np} t_{np}\right), \tag{3}$$

and:

$$m_2 = w\rho_{np} t_{np}. \tag{4}$$

Assuming the vibration is harmonic with time with an angular frequency ω, the axial displacement at any position x and time t, $H(x,t)$, can be written as $H(x,t) = h(x)e^{i\omega t}$ where $h(x)$ represents the axial vibration amplitude at position, x. We also have assumed that the length and width of the cantilever are much larger than the thickness, and that the transverse shear force is negligible so the Euler Bernoulli theory is valid. Damping also is neglected in the present treatment. The differential equation that governs $h(x)$ then can be simplified as [20], [21]:

$$D(x)\frac{d^4 h(x)}{dx^4} - m(x)\omega^2 h(x) = 0, \tag{5}$$

where $D(x)$ and $m(x)$ are the bending modulus and mass per unit length of the cantilever at position, x. For a cantilever with a thin extension as depicted in Fig. 2, $D(x) = D_1$ and $m(x) = m_1$ in section 1 and $D(x) = D_2$ and $m(x) = m_2$ in section 2. The general solutions that satisfy (5) have the following form:

$$h(x) = C_{11}\sin(k_1 x) + C_{12}\cos(k_1 x) + C_{13}\sinh(k_1 x) + C_{14}\cosh(k_1 x), \quad \text{for section 1,} \tag{6}$$

$$h(x) = C_{21}\sin(k_2 x) + C_{22}\cos(k_2 x) + C_{23}\sinh(k_2 x) + C_{24}\cosh(k_2 x), \quad \text{for section 2.} \tag{7}$$

The clamp boundary conditions at $x = -l_1$ requires that:

$$h = 0, \quad \text{at } x = -l_1, \tag{8}$$

and:

$$\frac{dh}{dx} = 0, \quad \text{at } x = -l_1. \tag{9}$$

At $x = l_2$, the free end boundary condition requires that the bending moment and the shear force be equal to 0, i.e.:

$$\frac{d^2 h}{dx^2} = 0, \quad \text{at } x = l_2, \tag{10}$$

and:

$$\frac{d^2 h}{dx^3} = 0, \quad \text{at } x = l_2. \tag{11}$$

At the boundary between section 1 and section 2 (i.e., $x = 0$) that the axial displacement (vibration amplitude),

the first derivative of the axial displacement, the bending moment, and the shear force must be continuous requires that:

$$h(x=0,\sec 1) = h(x=0,\sec 2), \tag{12}$$

$$\left.\frac{dh}{dx}\right|_{x=0,\sec 1} = \left.\frac{dh}{dx}\right|_{x=0,\sec 2}, \tag{13}$$

$$D_1 \left.\frac{d^2h}{dx^2}\right|_{x=0,\sec 1} = D_2 \left.\frac{d^2h}{dx^2}\right|_{x=0,\sec 2}, \tag{14}$$

and:

$$D_1 \left.\frac{d^3h}{dx^3}\right|_{x=0,\sec 1} = D_2 \left.\frac{d^3h}{dx^3}\right|_{x=0,\sec 2}. \tag{15}$$

Let:

$$a \equiv \frac{D_1}{D_2}, \tag{16}$$

and:

$$b \equiv \frac{k_1}{k_2}. \tag{17}$$

Because both section 1 and section 2 vibrate with the same frequency, ω, from (5), it follows that:

$$\omega^2 = \frac{D_1}{m_1}k_1^4 = \frac{D_2}{m_2}k_2^4. \tag{18}$$

Therefore, the wave vectors in section 1 and section 2 obey the following relationship:

$$b \equiv \frac{k_1}{k_2} = \sqrt[4]{\frac{D_2}{D_1}}\sqrt[4]{\frac{m_1}{m_2}}. \tag{19}$$

Eq. (19) indicates that, for any flexural vibration, the ratio, b, between the two wave vectors, k_1 and k_2 is fixed by the ratios, D_1/D_2 and m_1/m_2, which depend only on the material constants and geometry of the cantilever. Defining X_{11}, X_{12}, X_{21}, and X_{22} as in (20)–(23) (see next page). Using the boundary conditions, (8)–(15), and the expressions (16)–(23), we can obtain the expressions of seven of the eight coefficients C_{11}, $C_{12}, \ldots$ in terms of the eighth one as shown in (24)–(31) (see next page). Eqs. (26) and (27) lead to the transcendental equation:

$$\frac{X_{11}}{X_{12}} = \frac{X_{21}}{X_{22}}, \tag{32}$$

or (33) (see next page). Because a, b, l_1, and l_2 are constants that depend only on the materials and geometry of the cantilever, (32) or (33) can be solved numerically to obtain the eigen values, $k_{2,n}$ for the wave vector, k_2 where $n = 1, 2, 3, \ldots$ denotes the n^{th} mode. The n^{th}-mode eigen value, $k_{1,n}$, for k_1 and the n^{th}-mode resonance frequency $f_{r,n} = \omega_{r,n}/2\pi$, then can be obtained, respectively, using (19) and (18). The coefficients for the n^{th}-mode axial vibration amplitude, $h_n(x)$, then can be obtained numerically in terms of C_{14} using the expressions depicted in (24)–(31). Note that, when $l_1 = 0$ ($l_2 = 0$), the cantilever becomes one with a uniform cross section, (33) becomes:

$$\cosh(k_2 l_2)\cos(k_2 l_2) = -1, \quad \text{for } l_1 = 0, \tag{34}$$

and:

$$\cosh(k_1 l_1)\cos(k_1 l_1) = -1, \quad \text{for } l_2 = 0, \tag{35}$$

as expected for a uniform-cross-sectioned cantilever of length l_2 and l_1, respectively.

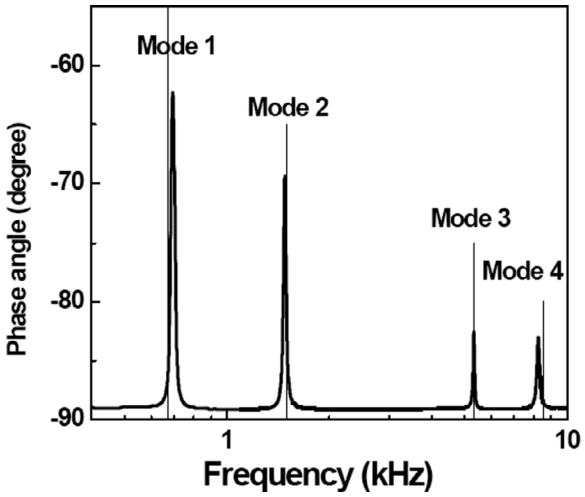

Fig. 3. Phase-angle-versus-frequency spectrum of a 12-mm long piezoelectric cantilever with an 8-mm long stainless steel extension. The vertical lines denote the calculated resonance frequencies.

IV. Results and Discussions

Fig. 3 shows the phase-angle-versus-frequency resonance spectrum of a PZT/stainless steel cantilever with a stainless steel extension in which section 1 had a PZT layer 12-mm long, 4-mm wide, 0.25-mm thick bonded to a stainless steel layer 0.07-mm thick and the stainless steel extension was 8-mm long. Off resonance, the cantilever behaved as a capacitor exhibiting a phase angle of $-90°$. At resonance, the flexural motion gave rise to a peak in the real part of the impedance. And, hence, a peak in the phase angle. Denoting the n^{th}-mode resonance frequency as $f_{r,n}$, the four resonance peaks were $f_{r,n} = 708$, 1520, 5400, and 8440 Hz, for $n = 1$, 2, 3, and 4, respectively. All four peaks had $Q_n \cong 50$ where $Q_n \equiv f_{r,n}/\Delta f_{r,n}$ with $f_{r,n}$ and $\Delta f_{r,n}$ denoting the peak frequency and peak width at half the peak height of the n^{th}-mode resonance, respectively. The ratios $f_{r,n}/f_{r,1}$ were, respectively, 2.2, 8.0, and 12.2, for $n = 2$, 3, and 4. Clearly, these ratios were very different from the values, 6.27, 17.55, and 34.39 known for a cantilever with a uniform cross section [14], [20], [21].

From the transcendental equation for cantilevers with an extension, (33), we can see the n^{th}-mode eigen values, $k_{1,n}$, $k_{2,n}$, are related to D_1, D_2, m_1, m_2, l_1, and l_2. Because the ratios D_1/D_2, m_1/m_2, and l_1/l_2 can be arbitrary,

$$
\begin{aligned}
X_{11} \equiv & \left[b(1-ab^2)\sinh(k_2l_2) - b(1+ab^2)\sin(k_2l_2)\right]\left[\sinh(k_1l_1)\cos(k_1l_1) + \cosh(k_1l_1)\sin(k_1l_1)\right] \\
& + \left[(1-ab^2)\cosh(k_2l_2) - (1+ab^2)\cos(k_2l_2)\right]\left[\sinh(k_1l_1)\sin(k_1l_1) - \cosh(k_1l_1)\cos(k_1l_1)\right] \\
& + \left[(1+ab^2)\cosh(k_2l_2) - (1-ab^2)\cos(k_2l_2)\right], \qquad (20) \\
X_{12} = & \left[b(1-ab^2)\sinh(k_2l_2) - b(1+ab^2)\sin(k_2l_2)\right]\left[\sinh(k_1l_1)\sin(k_1l_1) + \cosh(k_1l_1)\cos(k_1l_1)\right] \\
& + \left[(1-ab^2)\cosh(k_2l_2) - (1+ab^2)\cos(k_2l_2)\right]\left[\cosh(k_1l_1)\sin(k_1l_1) - \sinh(k_1l_1)\cos(k_1l_1)\right] \\
& + \left[b(1-ab^2)\sin(k_2l_2) - b(1+ab^2)\sinh(k_2l_2)\right], \qquad (21) \\
X_{21} = & \left[b(1-ab^2)\cosh(k_2l_2) - b(1+ab^2)\cos(k_2l_2)\right]\left[\sinh(k_1l_1)\cos(k_1l_1) + \cosh(k_1l_1)\sin(k_1l_1)\right] \\
& + \left[(1-ab^2)\sinh(k_2l_2) + (1+ab^2)\sin(k_2l_2)\right]\left[\sinh(k_1l_1)\sin(k_1l_1) - \cosh(k_1l_1)\cos(k_1l_1)\right] \\
& + \left[(1+ab^2)\sinh(k_2l_2) + (1-ab^2)\sin(k_2l_2)\right], \qquad (22) \\
X_{22} = & \left[b(1-ab^2)\cosh(k_2l_2) - b(1+ab^2)\cos(k_2l_2)\right]\left[\sinh(k_1l_1)\sin(k_1l_1) + \cosh(k_1l_1)\cos(k_1l_1)\right] \\
& + \left[(1-ab^2)\sinh(k_2l_2) + (1+ab^2)\sin(k_2l_2)\right]\left[\cosh(k_1l_1)\sin(k_1l_1) - \sinh(k_1l_1)\cos(k_1l_1)\right] \\
& + \left[b(1-ab^2)\cos(k_2l_2) - b(1+ab^2)\cosh(k_2l_2)\right]. \qquad (23)
\end{aligned}
$$

$$\frac{C_{11}}{C_{14}} = \frac{X_{11}}{X_{12}}\left[-\sinh(kl_1)\sin(kl_1) - \cosh(kl_1)\cos(kl_1)\right] + \left[\sinh(kl_1)\cos(kl_1) + \cosh(kl_1)\sin(kl_1)\right], \qquad (24)$$

$$\frac{C_{12}}{C_{14}} = \frac{X_{11}}{X_{12}}\left[\sinh(kl_1)\cos(kl_1) - \cosh(kl_1)\sin(kl_1)\right] + \left[\sinh(kl_1)\sin(kl_1) - \cosh(kl_1)\cos(kl_1)\right], \qquad (25)$$

$$\frac{C_{13}}{C_{14}} = \frac{X_{11}}{X_{12}}, \qquad (26)$$

$$\frac{C_{13}}{C_{14}} = \frac{X_{21}}{X_{22}}, \qquad (27)$$

$$\frac{C_{21}}{C_{14}} = \frac{1}{2}b(1+ab^2)\left\{\begin{array}{l}\left[-\sinh(kl_1)\sin(kl_1) - \cosh(kl_1)\cos(kl_1)\right]\frac{X_{11}}{X_{12}} \\ \quad + \left[\sinh(kl_1)\cos(kl_1) + \cosh(kl_1)\sin(kl_1)\right]\end{array}\right\} + \frac{1}{2}b(1-ab^2)\frac{X_{11}}{X_{12}}, \qquad (28)$$

$$\frac{C_{22}}{C_{14}} = \frac{1}{2}(1+ab^2)\left\{\begin{array}{l}\left[\sinh(kl_1)\cos(kl_1) - \cosh(kl_1)\sin(kl_1)\right]\frac{X_{11}}{X_{12}} \\ \quad + \left[\sinh(kl_1)\sin(kl_1) - \cosh(kl_1)\cos(kl_1)\right]\end{array}\right\} + \frac{1}{2}(1-ab^2), \qquad (29)$$

$$\frac{C_{23}}{C_{14}} = \frac{1}{2}b(1-ab^2)\left\{\begin{array}{l}\left[-\sinh(kl_1)\sin(kl_1) - \cosh(kl_1)\cos(kl_1)\right]\frac{X_{11}}{X_{12}} \\ \quad + \left[\sinh(kl_1)\cos(kl_1) + \cosh(kl_1)\sin(kl_1)\right]\end{array}\right\} + \frac{1}{2}b(1+ab^2)\frac{X_{11}}{X_{12}}, \qquad (30)$$

$$\frac{C_{24}}{C_{14}} = \frac{1}{2}(1-ab^2)\left\{\begin{array}{l}\left[\sinh(kl_1)\cos(kl_1) - \cosh(kl_1)\sin(kl_1)\right]\frac{X_{11}}{X_{12}} \\ \quad + \left[\sinh(kl_1)\sin(kl_1) - \cosh(kl_1)\cos(kl_1)\right]\end{array}\right\} + \frac{1}{2}(1+ab^2). \qquad (31)$$

$$
\begin{aligned}
& \frac{\left\{\begin{array}{l}\left[b(1-ab^2)\sinh(k_2l_2) - b(1+ab^2)\sin(k_2l_2)\right]\left[\sinh(k_1l_1)\cos(k_1l_1) + \cosh(k_1l_1)\sin(k_1l_1)\right] \\ + \left[(1-ab^2)\cosh(k_2l_2) - (1+ab^2)\cos(k_2l_2)\right]\left[\sinh(k_1l_1)\sin(k_1l_1) - \cosh(k_1l_1)\cos(k_1l_1)\right] \\ + \left[(1+ab^2)\cosh(k_2l_2) - (1-ab^2)\cos(k_2l_2)\right]\end{array}\right\}}{\left\{\begin{array}{l}\left[b(1-ab^2)\sinh(k_2l_2) - b(1+ab^2)\sin(k_2l_2)\right]\left[\sinh(k_1l_1)\sin(k_1l_1) + \cosh(k_1l_1)\cos(k_1l_1)\right] \\ + \left[(1-ab^2)\cosh(k_2l_2) - (1+ab^2)\cos(k_2l_2)\right]\left[\cosh(k_1l_1)\sin(k_1l_1) - \sinh(k_1l_1)\cos(k_1l_1)\right] \\ + \left[b(1-ab^2)\sin(k_2l_2) - b(1+ab^2)\sinh(k_2l_2)\right]\end{array}\right\}}, \\
& = \frac{\left\{\begin{array}{l}\left[b(1-ab^2)\cosh(k_2l_2) - b(1+ab^2)\cos(k_2l_2)\right]\left[\sinh(k_1l_1)\cos(k_1l_1) + \cosh(k_1l_1)\sin(k_1l_1)\right] \\ + \left[(1-ab^2)\sinh(k_2l_2) + (1+ab^2)\sin(k_2l_2)\right]\left[\sinh(k_1l_1)\sin(k_1l_1) - \cosh(k_1l_1)\cos(k_1l_1)\right] \\ + \left[(1+ab^2)\sinh(k_2l_2) + (1-ab^2)\sin(k_2l_2)\right]\end{array}\right\}}{\left\{\begin{array}{l}\left[b(1-ab^2)\cosh(k_2l_2) - b(1+ab^2)\cos(k_2l_2)\right]\left[\sinh(k_1l_1)\sin(k_1l_1) + \cosh(k_1l_1)\cos(k_1l_1)\right] \\ + \left[(1-ab^2)\sinh(k_2l_2) + (1+ab^2)\sin(k_2l_2)\right]\left[\cosh(k_1l_1)\sin(k_1l_1) - \sinh(k_1l_1)\cos(k_1l_1)\right] \\ + \left[b(1-ab^2)\cos(k_2l_2) - b(1+ab^2)\cosh(k_2l_2)\right]\end{array}\right\}}.
\end{aligned} \qquad (33)
$$

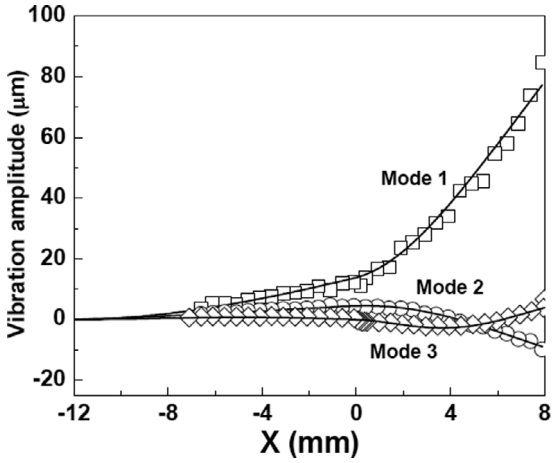

Fig. 4. Resonance vibration amplitude versus x (location) of the 12-mm long piezoelectric cantilever with an 8-mm long stainless steel extension shown in Fig. 3. The solid lines represent calculated resonance vibration amplitudes as described in the text.

it is conceivable that the ratios, $f_{r,n}/f_{r,1}$, can depend on the ratios of D_1/D_2, m_1/m_2, and l_1/l_2, and thus can be utterly different from those of a uniform-cross-sectioned cantilever. Given the cantilever dimensions and the material constants given in Table I, we solved the transcendental equation (33) and obtained 671 Hz, 1502 Hz, 5334 Hz, and 8552 Hz as the theoretical resonance frequencies. The theoretical ratios of the n^{th}-mode resonance frequencies to the first-mode resonance frequency, $f_{r,n}/f_{r,1}$, were 2.24, 7.94, and 12.75 for $n = 2$, 3, and 4, respectively. As can be seen, the calculated resonance frequencies and the theoretical ratios, $f_{r,n}/f_{r,1}$ compared well with the experimental values with a relative difference equal to or less than 5% for all four modes, likely a result neglecting the glue layer and the damping effect. That the theoretical resonance frequencies agree well with the experimental values and that the resultant $f_{r,n}/f_{r,1}$ were very different from those expected from a uniform-cross-sectioned cantilever indicated that the present model which allowed different bending moduli and masses per unit length in different sections of a cantilever indeed captured the essential physics of a piezoelectric cantilever with an extension.

Fig. 4 shows the measured resonance vibration amplitudes, $h_{1,\exp}(x)$ of Mode 1 (open square), $h_{2,\exp}(x)$ of Mode 2 (open circles), and $h_{3,\exp}(x)$ of Mode 3 (open triangles) of the cantilever whose resonance spectrum was shown in Fig. 3. The resonance displacements, $h_{1,\exp}(x)$, $h_{2,\exp}(x)$, and $h_{3,\exp}(x)$ were measured with an applied voltage of 0.5 V at 708 Hz, 1520 Hz, and 5400 Hz, respectively. Note that the resonance vibration or displacement amplitude for cantilevers with an extension showed considerable "distortion" from that of a uniform-cross-sectioned cantilever, most notably, an enhancement of the displacement amplitude toward the free end of the stainless steel extension. The distortion was particularly clear in Mode 2 and Mode 3 resonance displacement amplitudes, $h_{2,\exp}(x)$ and $h_{3,\exp}(x)$. The higher displacement amplitude toward the end of the stainless extension was attributed to the fact that the stainless steel extension (section 2) was thinner and less stiff than section 1. Theoretically, $h_{n,th}(x)$ was calculated using the expressions for the coefficients depicted in (24)–(31) with C_{14} as an adjustable parameter. The value of C_{14} was chosen such that $h_{n,th}(x = 12\text{ mm}) = h_{n,\exp}(x = 12\text{ mm})$. From Fig. 4, we can see that the theoretical $h_{n,th}(x)$ agreed well with the experimental $h_{n,\exp}(x)$. The good agreement between the $h_{n,th}(x)$ and the $h_{n,\exp}(x)$ and the agreement for the enhancement in the displacement amplitude toward the end of the stainless steel extension further validated the current theory that took into account the difference in the bending moduli and masses per unit length between the two sections and that it had the accurate expression for the bending modulus of section 1.

The effect of l_1 was examined with the stainless-steel extension length, l_2 fixed and by varying the length of section 1, l_1. The thickness of the PZT and that of the stainless steel were the same as those in Figs. 3 and 4. The resultant measured and calculated resonance frequencies for $l_2 = 6$ mm and $l_2 = 4$ mm for various l_1 are plotted in Fig. 5(a) and (b), respectively. As can be seen in both cases, the resonance frequency increased with a decreasing l_1 and all the measured resonance frequencies were in good agreement with the calculated resonance frequencies, validating the calculations.

From (18), we can see that $f_{r,n}/k_{i,n}^2 = \sqrt{m_i/D_i}$ where $i = 1$ or 2, denoting section 1 or 2 and n the mode. To show that the model is general and works for all conditions, we summarize in Fig. 6 all the results shown in Figs. 3–5 in the form of $f_{r,n,\exp}/k_{i,n}^2$ versus l_1/l_2, where $i = 1$ or 2, denoting the section, and $n = 1$, 2, or 3 denoting the mode. One can see that, for l_1/l_2, both smaller and larger than one and for all resonance modes, $f_{r,n,\exp}/k_{1,n}^2$ of section 1 and $f_{r,n,\exp}/k_{2,n}^2$ of section 2 collapsed on the solid lines that represent the numerical values of $\sqrt{m_1/D_1}$ and $\sqrt{m_2/D_2}$, respectively, indicating that the present model indeed represents a two-sectioned piezoelectric cantilever in a general form.

A. Effect of l_1/l_2 on $f_{r,n}/f_{r,1}$

From the above results, we can see that, unlike cantilevers with a uniform thickness that have fixed $f_{r,n}/f_{r,1}$ ratios where $n = 2, 3, \ldots$, cantilevers with two distinctive sections of different thickness/bending moduli can have varying $f_{r,2}/f_{r,1}$ and $f_{r,3}/f_{r,1}$ ratios that depend on the dimensions and physical parameters of each section. A summary of the dependence of $f_{r,2}/f_{r,1}$ and $f_{r,3}/f_{r,1}$ on l_1/l_2 is shown in Fig. 7 where we plot $f_{r,2}/f_{r,1}$ versus l_1/l_2 and $f_{r,3}/f_{r,1}$ versus l_1/l_2, respectively. The solid lines represent the calculated values and the full squares the experimental data. Fig. 7 shows that $f_{r,2}/f_{r,1}$ ($f_{r,3}/f_{r,1}$) underwent a minimum (minima) at intermediate l_1/l_2 and approached a constant value at both $l_1/l_2 \ll 1$ and $l_1/l_2 \gg 1$, which was borne out by the experimental data (full squares). For the cantilevers we studied in this paper, the minimum value of $f_{r,2}/f_{r,1}$ was about 2.2 and occurred at $l_1/l_2 = 1.8$,

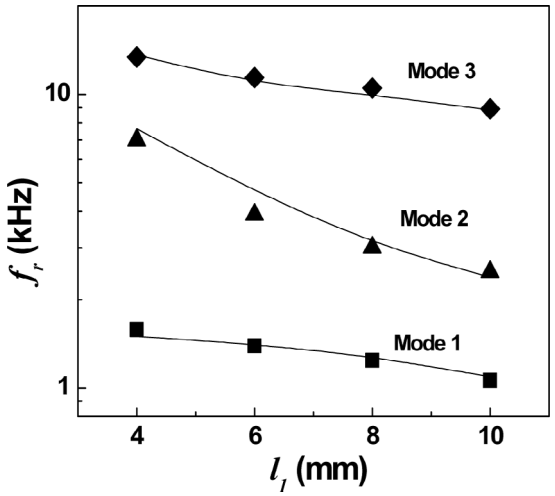

(a)

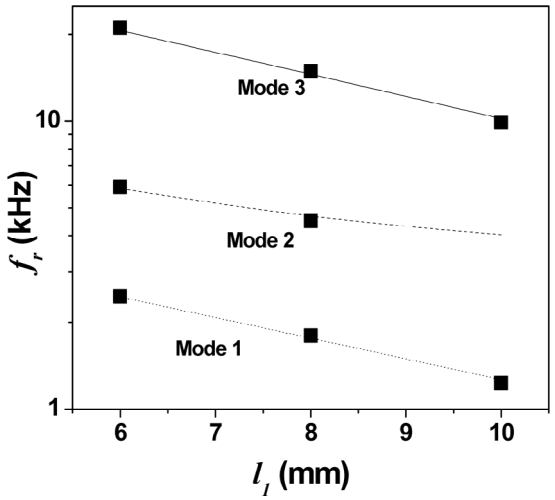

(b)

Fig. 5. Resonance frequency versus l_1 for (a) $l_2 = 6$ mm; (b) $l_2 = 4$ mm where solid squares, solid triangles, and solid diamonds denote modes 1, 2, and 3, respectively. The solid lines represent calculated resonance frequencies.

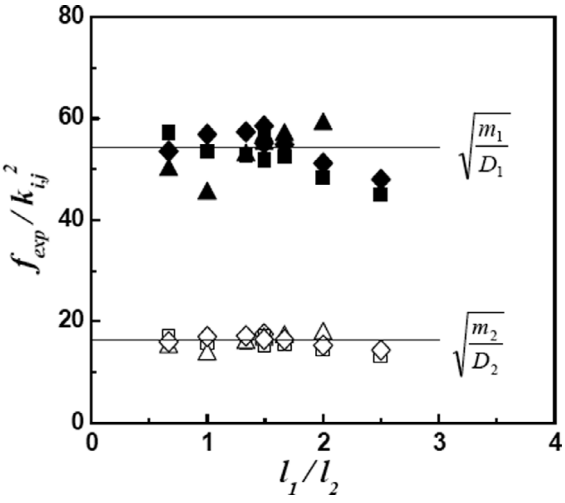

Fig. 6. f_{exp}/k_1^2 (solid symbols) and f_{exp}/k_2^2 (open symbols) versus l_1/l_2 for all the cantilevers shown in Figs. 3–5. Squares, triangles, and diamonds represent modes 1, 2, and 3, respectively. The solid lines represent $\sqrt{m_i/D_i}$ with $i = 1$ or 2 as described in the text.

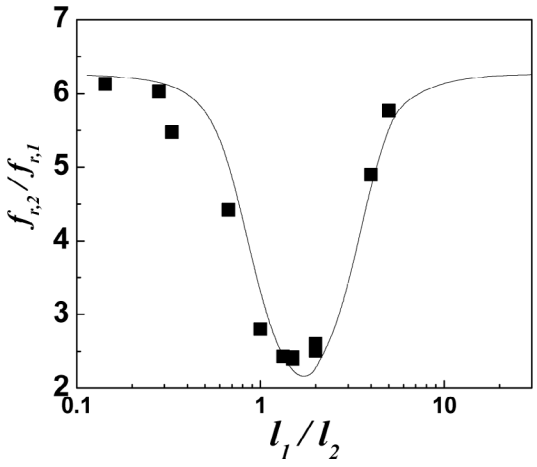

(a)

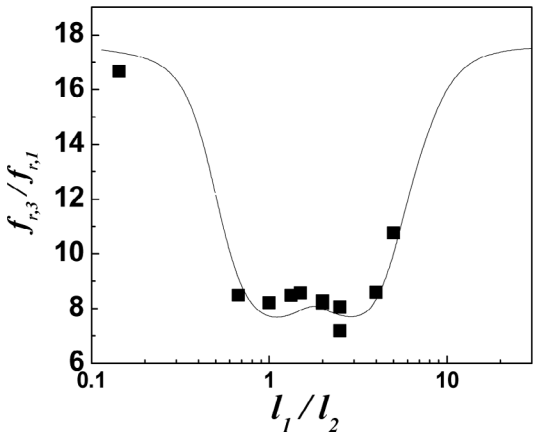

(b)

Fig. 7. (a) $f_{r,2}/f_{r,1}$ versus l_1/l_2 and (b) $f_{r,3}/f_{r,1}$ versus l_1/l_2 where the solid squares represent the measured resonance frequency ratio and the solid lines denote the calculated values.

and the minima of $f_{r,3}/f_{r,1}$ were about 8 and occurred at $l_1/l_2 = 1$ and $l_1/l_2 = 2.5$. The ratios $f_{r,2}/f_{r,1}$ and $f_{r,3}/f_{r,1}$, respectively, approached 6.27 and 17.6 at both $l_1/l_2 \ll 1$ and $l_1/l_2 \gg 1$ because at $l_1/l_2 \ll 1$ ($l_1/l_2 \gg 1$), the two-sectioned cantilever asymptotically approaches a cantilever of uniform thickness of length $l_2(l_1)$.

B. Effect of l_1/l_2 on $I_{r,2}/I_{r,1}$

Another characteristic of piezoelectric cantilevers with a nonpiezoelectric extension is that their highest resonance peak may not always occur at the first mode, which is unlike cantilevers of a uniform cross section. We plot the experimental peak height ratio, I_2/I_1, versus l_1/l_2 (full squares) in Fig. 8(a) where I_2 and I_1 represent the second and first resonance peak heights, respectively. Also shown in Fig. 8(a) are the asymptotic peak height ratio, $I_2/I_1 = 1/6.24$ at $l_1/l_2 = \infty$ (open square). Clearly, there are two regions. In region I where $l_1/l_2 \geq 1.5$, I_2/I_1 was always smaller than unity. In region II where $l_1/l_2 \leq 1.5$, I_2/I_1 could be larger than unity and peaked around $l_1/l_2 = 0.6$. Examples of spectra in region I in which the first peak was always higher than the second peak are shown in Fig. 9(a) with cantilevers of a 8-mm and

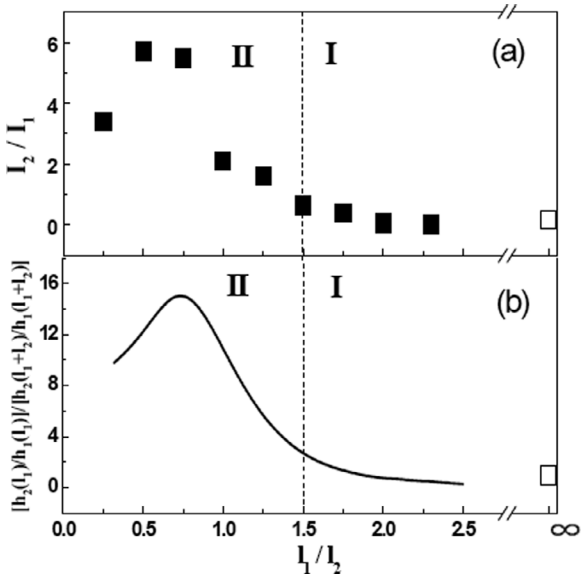

Fig. 8. (a) The measured peak height ratio of Mode 2 to Mode 1 and (b) the calculated $[h_2(l_1)/h_1(l_1)]/[h_2(l_1+l_2)/h_1(l_1+l_2)]$ versus l_1/l_2.

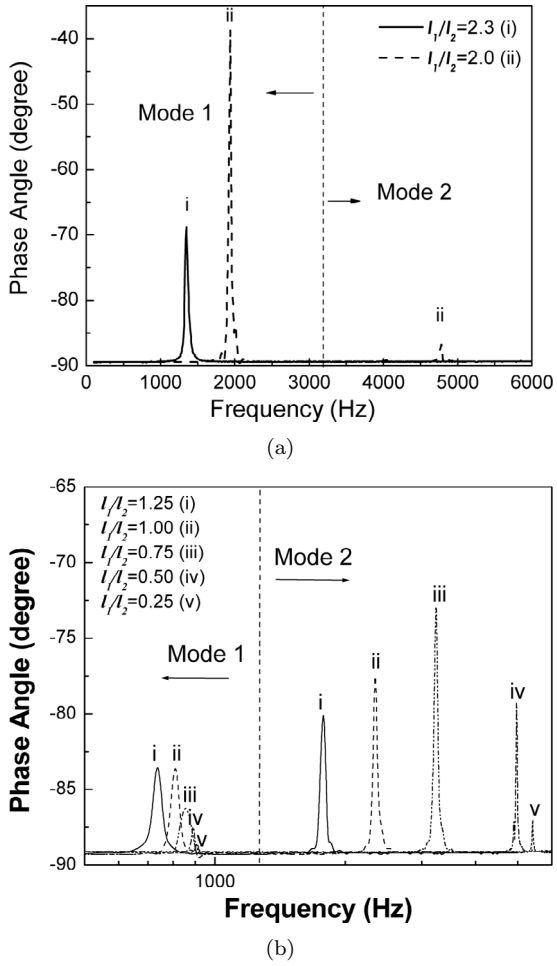

Fig. 9. (a) Phase-angle-versus-frequency of cantilevers with l_1/l_2, ≥ 1.5 [$l_2 = 4$ mm and $l_1 = 8$ mm (solid line), 9.2 mm (dash line)]. (b) That of cantilevers with $l_1/l_2 \leq 1.5$ [$l_2 = 8$ mm and $l_1 = 10$ mm (i), 8 mm (ii), 6 mm (iii), 4 mm (iv), and 2 mm (v)], respectively.

9.2-mm PZT section and a 4-mm nonpiezoelectric extension length ($l_1/l_2 = 2.0$ and 2.3, respectively). Examples of spectra in region II are shown in Fig. 9(b) with cantilevers of a 2-mm, 4-mm, 6-mm, 8-mm, and 10-mm PZT section, respectively, and an 8-mm nonpiezoelectric extension length (l_1/l_2 ranging 0.25–1.25). Clearly, as can be seen from Figs. 8(a), 9(a) and (b), the ratio l_1/l_2 played an important role in determining the resonance peak intensity ratio. This came about because the resonance electrical impedance signals were solely determined by the vibration amplitude within the piezoelectric layer. How the peak height of a higher-mode resonance compared to the peak height of the first-mode depended mainly on how the higher-mode vibration amplitude within the piezoelectric layer compared to that of the first mode, which could be strongly affected by the ratio of the length of the piezoelectric section to that of the nonpiezoelectric extension, l_1/l_2. To illustrate this point, we plot the calculated $h_1(x)$ and $h_2(x)$ versus x in Fig. 10(a) for the cantilever with $l_1 = 9.2$ mm and $l_2 = 4$ mm ($l_1/l_2 = 2.3$) whose spectrum was shown as the solid line in Fig. 9(a) and that for the cantilever with $l_1 = 6$ mm and $l_2 = 8$ mm ($l_1/l_2 = 0.75$) whose spectrum was shown in Fig. 9(b) as the dash line, respectively. From Fig. 10(a), it can be seen that second-mode vibration amplitude, $h_2(x)$ exhibited a nodal point near $x = 0$. Note that the second peak of this cantilever was absent in Fig. 9(a) as consistent with the presence of the nodal point at $x = 0$ shown in Fig. 10(a) which indicated that there was little bending stress and, therefore, little induced piezoelectric voltage near $x = 0$. In contrast, for $l_1/l_2 = 0.75$, the second-mode vibration amplitude within the piezoelectric section ($x \leq l_1$) was higher than that of the first mode, indicating a higher stress and hence a higher piezoelectric response, although the first-mode vibration amplitude was higher than the second mode toward the free end ($x = l_1 + l_2$) of the nonpiezoelectric extension section. As a summary, we plot the calculated, normalized vibration amplitude ratio, $[h_2(l_1)/h_1(l_1)]/[h_2(l_1 + l_2)/h_1(l_1 + l_2)]$ as the solid curve in Fig. 8(b) to compare with the experimental peak height ratio, I_2/I_1 in Fig. 8(a). Clearly, the normalized vibration amplitude ratio, $[h_2(l_1)/h_1(l_1)]/[h_2(l_1+l_2)/h_1(l_1+l_2)]$ versus l_1/l_2 exhibited a peak around $l_1/l_2 = 0.6$, as similar to the experimental peak height ratio, I_2/I_1 shown in Fig. 8(a), indicating that the resonance peak height is closely related to the relative vibration amplitude of the PZT part (as normalized by the amplitude at the free end).

It would be of great interest to compare the current analytical model with existing numerical finite element method (FEM) models. We are not aware of any FEM models that have the same geometry as that studied by the current analytical model. To go further and predict the quantitative behavior of vibration amplitude and resonance peak height ratio, we must consider the vibration of the cantilevers under a driving condition. In the future, we will investigate the theory for vibration behavior under driving conditions using a FEM model.

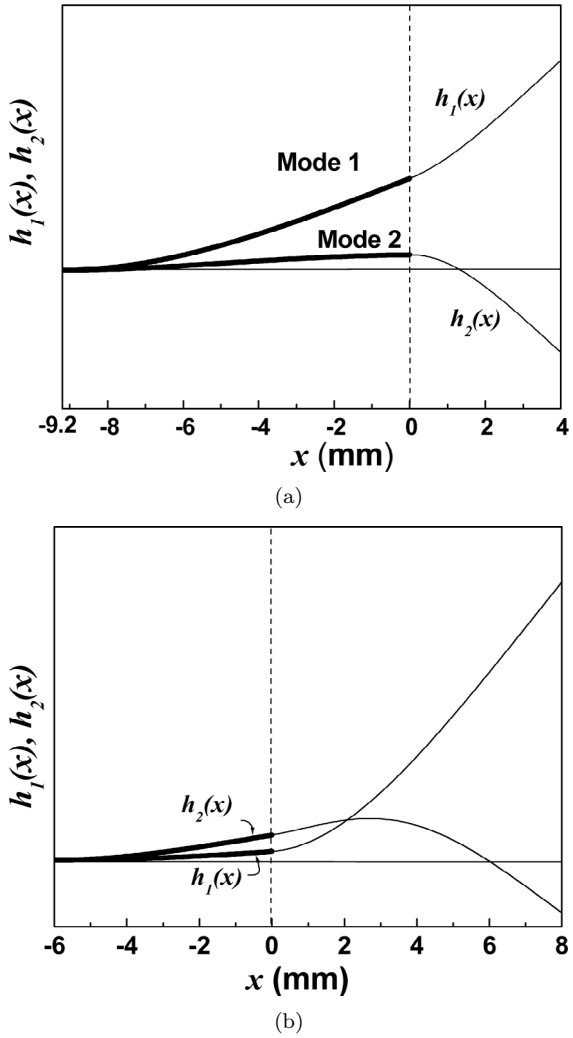

Fig. 10. The calculated $h_1(x)$ and $h_2(x)$ versus x for (a) the cantilever with $l_1 = 9.2$ mm and $l_2 = 4$ mm ($l_1/l_2 = 2.3$) and that of (b) the cantilever with $l_1 = 6$ mm and $l_2 = 8$ mm ($l_1/l_2 = 0.75$), respectively.

V. Conclusions

For the practical need of a probe to be dipped into liquid for sensing applications as well as the benefits of added flexibility, a piezoelectric cantilever sensor with a nonpiezoelectric extension was studied. We have examined both experimentally and theoretically the resonance behavior of piezoelectric cantilevers with a nonpiezoelectric extension of various lengths and length ratios between the two sections. Experimentally, piezoelectric cantilevers of various length and various length ratios between the nonpiezoelectric extension section and the piezoelectric section were constructed, and their resonance spectra and resonance vibration waveforms were examined. Theoretically, an analytic transcendental equation was derived that was solved numerically to obtain resonance frequencies and vibration waveforms to compare with experimental results. Both the theoretical and experimental results showed that the presence of a nonpiezoelectric extension distorted the flexural vibration waveforms from those of cantilevers of a uniform thickness. As a result, it also changed the resonance frequency ratios and the peak intensity ratios between different resonance modes. For a PEC with a 0.25-mm thick PZT layer and a 0.07-mm thick stainless steel layer, the first-mode-to-second-mode resonance frequency ratio exhibited a minimum of about 2.2 at $l_1/l_2 = 1.8$, and the first-mode-to-second-mode resonance peak intensity ratio showed a maximum of 5.6 at $l_1/l_2 = 0.75$.

References

[1] J. H. Lee, K. H. Yoon, D. S. Yoon, J. Park, S. Ahn, and T. S. Kim, "Label free novel electrical detection using micromachined PZT monolithic thin film cantilever for the detection of C-reactive protein," *Biosens. Bioelectron.*, vol. 20, pp. 269–275, 2004.

[2] J. H. Lee, K. S. Hwang, J. Park, K. H. Yoon, D. S. Yoon, and T. S. Kim, "Immunoassay of prostate-specific antigen (PSA) using resonant frequency shift of piezoelectric nanomechanical microcantilever," *Biosens. Bioelectron.*, vol. 20, pp. 2157–2162, 2005.

[3] K. S. Hwang, J. H. Lee, J. Park, D. S. Yoon, J. H. Park, and T. S. Kim, "*In-situ* quantitative analysis of a prostate-specific antigen (PSA) using a nanomechanical PZT cantilever," *Lab. Chip.*, vol. 4, pp. 547–552, 2004.

[4] J. W. Yi, W. Y. Shih, R. Mutharasan, and W.-H. Shih, "In situ cell detection using piezoelectric lead zirconate titanate-stainless steel cantilevers," *J. Appl. Phys.*, vol. 93, pp. 619–625, 2003.

[5] W. Y. Shih, G. Campbell, J. W. Yi, R. Mutharasan, and W. H. Shih, "Ultrasensitive pathogen quantification in drinking water using highly piezoelectric microcantilevers," in *Nanotechnology and the Environment—Applications and Implications*. B. Karn, T. Masciangioli, W.-X. Zhang, V. Colvin, and P. Alivasatos, Eds. London: Oxford Univ. Press, 2004, ch. 23, pp. 179–185.

[6] C. S. Kim, R. J. Lad, and C. P. Tripp, "Interaction of organophosphorous compounds with TiO_2 and WO_3 surfaces probed by vibrational spectroscopy," *Sens. Actuators B, Chem.*, vol. 76, pp. 442–448, 2001.

[7] S. W. Oh, Y. H. Kim, D. J. Yoo, S. M. Oh, and S. J. Park, "Sensing behavior of semiconducting metal-oxide for the detection of organophosphorus compounds," *Sens. Actuators B*, vol. 13–14, pp. 400–403, 1993.

[8] L. A. Pinnaduwage, V. Boiadjiev, J. E. Hawk, and T. Thundat, "Sensitive detection of plastic explosives with self-assembled monolayer-coated microcantilevers," *Appl. Phys. Lett.*, vol. 83, pp. 1471–1473, 2003.

[9] B. H. Kim, F. E. Prins, D. P. Kern, S. Raible, and U. Weimar, "Multicomponent analysis and prediction with a cantilever array based gas sensor," *Sens. Actuators B, Chem.*, vol. 78, pp. 12–18, 2001.

[10] Q. Zhao, W. Y. Shih, and W.-H. Shih, "Microporous-SiO_2-coated piezoelectric cantilever sensor for dimethyl methylphosphonate (DMMP) detection," *Sens. Actuators, B, Chem.*, vol. 117, pp. 74–79, 2006.

[11] G. Li, L. W. Burggraf, and W. P. Baker, "Photothermal spectroscopy using multilayer cantilever for chemical detection," *Appl. Phys. Lett.*, vol. 76, pp. 1122–1124, 2000.

[12] Z. Shen, W. Y. Shih, and W.-H. Shih, "Self-exciting, self-sensing PZT/SiO_2 piezoelectric micro-cantilever sensors with femtogram/Hz sensitivity," *Appl. Phys. Lett.*, vol. 89, art. no. 023506, 2006.

[13] T. G. Thundat and J. Adams, "The 2004 Scientific American 50 Award: Research Leaders," *Sci. Amer.*, vol. 291, p. 47, 2004.

[14] J. W. Yi, W. Y. Shih, and W.-H. Shih, "Effect of length, width, and mode on the mass detection sensitivity of piezoelectric unimorph cantilevers," *J. Appl. Phys.*, vol. 91, no. 3, pp. 1680–1686, 2002.

[15] W. Y. Shih, X. Li, H. Gu, W.-H. Shih, and I. A. Aksay, "Simultaneous liquid viscosity and density determination with piezoelectric unimorph cantilevers," *J. Appl. Phys.*, vol. 89, no. 2, pp. 1497–1505, 2001.

[16] W. Y. Shih, X. Li, J. Vartuli, D. L. Milius, R. Prud'homme, I. A. Aksay, and W.-H. Shih, "Detection of water-ice transition using

a lead zirconate titanate/brass transducer," *J. Appl. Phys.*, vol. 92, no. 1, pp. 106–111, 2002.
[17] C. Lee, T. Itoh, and T. Suga, "Self-excited piezoelectric PZT microcantilevers for dynamic SFM—With inherent sensing and actuating capabilities," *Sens. Actuators, A*, vol. 72, pp. 179–188, 1999.
[18] J. Fritz, M. K. Baller, H. P. Lang, H. Rothuizen, P. Vettiger, E. Meyer, H.-J. Guntherodt, C. Gerber, and J. K. Gimzewski, "Translating biomolecular recognition into nanomechanics," *Science*, vol. 288, pp. 316–318, 2000.
[19] P. I. Oden, G. Y. Chen, R. A. Steele, R. J. Warmack, and T. Thundat, "Viscous drag measurements utilizing microfabricated cantilevers," *Appl. Phys. Lett.*, vol. 68, pp. 3814–3816, 1996.
[20] J. Merhaut, *Theory of Electroacoustics*. New York: McGraw-Hill, 1981.
[21] C. de Silva, *Vibration, Fundamentals and Practice*. New York: CRC Press, 2002, p. 302.
[22] J. G. Smits and W.-S. Choi, "The constituent equations of piezoelectric heterogeneous bimorphs," *IEEE Trans. Ultrason., Ferroelect., Freq. Contr.*, vol. 38, no. 3, pp. 256–270, 1991.
[23] L. Tong and Q. Luo, "Exact dynamic solutions to piezoelectric smart beams including peel stresses I: Theory and application," *Int. J. Solids Struct.*, vol. 40, pp. 4789–4812, 2003.
[24] L. Cattafesta, III, S. Garg, and D. Shukla, "Development of piezoelectric actuators for active flow control," *AIAA J.*, vol. 39, pp. 1562–1568, 2001.

Zuyan Shen received his B.S. degree in physics in 1998, and M.S. degree in physics in 2001 from the Department of Physics at Wuhan University, Wuhan, China. He worked for New Focus Ltd., Shenzhen, China, as an R and D engineer for the development of optoelectronic devices from 2001 to 2002. He joined the Department of Materials Science and Engineering, at Drexel University, Philadelphia, PA, as a graduate student in the spring of 2002 and is currently a Ph.D. candidate in the department.

His studies at Drexel have focused on the general characterization and modeling of piezoelectric cantilever mass sensors as well as the synthesis and microfabrication of PZT/SiO_2 microcantilever sensors.

Wan Y. Shih is an associate professor in the School of Biomedical Engineering, Science, and Health Systems at Drexel University, Philadelphia, PA. She received her B.S. degree in physics in 1976 from Tsing-Hua University, Hsinchu, Taiwan and completed her Ph.D. degree in physics in 1984 from Ohio State University, Columbus, OH. After 1 year of postdoctoral research in the Materials Research Laboratory at Ohio State University, she was a research scientist in the Department of Materials Science and Engineering at the University of Washington, Seattle, WA, from 1985–1992. She became a research associate professor in the Department of Materials Science and Engineering at Drexel University in 1993. During the period 1993 and 1999 she also was a research scientist in the Princeton Materials Institute at Princeton University, Princeton, NJ.

Her research has covered a wide range of areas of materials science and applications, including colloidal ceramics, colloidal aggregation and stability, piezoelectric materials and devices, sensors, and actuators.

She has received the American Ceramic Society 1999 Edward C. Henry Electronics Division Best Paper Award in 1999. Her current research focuses on the development of portable array miniaturized piezoelectric sensors for biological and chemical sensing applications.

Wei-Heng Shih is a professor in the Department of Materials Science and Engineering at Drexel University, Philadelphia, PA. He received a B.Sc. degree in physics in 1976 from Tsing-Hua University, Hsinchu, Taiwan and completed his Ph.D. degree in physics in 1984 from Ohio State University, Columbus, OH. After postdoctoral research at University of Washington, Seattle, WA, in the Physics Department and Materials Science and Engineering Department, he joined Drexel University in 1991.

His research has covered a wide range of areas of materials science, including surface modification of powders by colloidal coating, sol-gel processing of microporous and mesoporous powders, low-temperature processing of perovskite piezoelectric ceramics, and fabrication of piezoelectric sensors. He has received the American Ceramic Society 1999 Edward C. Henry Electronics Division Best Paper Award and the Drexel's Research Achievement Award.

His current research focuses on the development of aqueous synthesis of nanocrystalline quantum dots, highly piezoelectric free-standing films, and lead-free piezoelectric ceramics for imaging and sensor applications.